JOURNAL OF THERMOPHYSICS AND HEAT TRANSFER
Vol. 7, No. 3, July–Sept. 1993

Cool-Down of a Vertical Line with Liquid Nitrogen

A. Hedayatpour* and B. N. Antar†
University of Tennessee Space Institute, Tullahoma, Tennessee 37388
and
M. Kawaji‡
University of Toronto, Toronto, Ontario, Canada

Analytical and numerical modeling is presented for predicting the thermofluid parameters of the cool-down process of an open-to-air vertical tube carrying liquid nitrogen. A two-fluid mathematical model is employed to describe the flowfield. In this model four distinct flow regions were analyzed: 1) fully liquid, 2) inverted annular film boiling, 3) dispersed flow, and 4) fully vapor. These flow regimes were observed in an experimental investigation constructed for validating the mathematical model, and also in previous experiments by other investigators. For the single-phase regions, the one-dimensional form of mass, momentum, and energy equations were used. For the two-phase regions, the volume-averaged, phasic one-dimensional form of conservation equations were applied. The one-dimensional energy equation was formulated to determine the tube wall temperature history. The numerical procedure is based on the semi-implicit, finite-difference technique. The calculations for the inverted annular film boiling were performed implicitly. The computations for the tube wall, fully liquid, and dispersed flow regions were performed explicitly. In each region, the appropriate models for heat transfer and shear stress rates are used. Results and comparisons of the predicted numerical models with the experimental data for several constant inlet flow rates of liquid nitrogen into a vertical, insulated tube are presented.

Nomenclature

A_w = cross-sectional area of the flow channel, m²
c_p = specific heat capacity, J/kg °C
D_a = area-averaged, population-mean diameter of drops, m
$D^e_{\max}$ = maximum entrainable diameter of drops, m
$D^s_{\max}$ = maximum stable diameter of drops, m
D_{smd} = Sauter mean diameter of a droplet population, m
D_v = volume averaged, population-mean diameter of drops, m
d = diameter of the flow channel, m
g = local acceleration of gravity, m/s²
h = enthalpy, J/kg
h_c = convective heat transfer coefficient, W/m² °C
h_{nb} = heat transfer coefficient for nucleate boiling, W/m² °C
$h_{,\text{sat}}$ = saturation enthalpy of either liquid or vapor, J/kg
k = thermal conductivity, W/m °C
L_{fg} = latent heat of vaporization, J/kg
m''' = interfacial mass transfer rate, kg/m³s
q'' = heat flux per unit area, W/m²
q''' = heat transfer rate per unit volume, W/m³
q''_{evap} = vaporization heat flux, W/m²
q''_{rad} = wall to liquid radiation, W/m²
q''^r_{vd} = vapor to drop radiation heat flux, W/m²
q''^r_{wd} = wall to drop radiation heat flux, W/m²
q''^r_{wv} = wall to vapor radiation heat flux, W/m²
Pi = inner perimeter of tubular flow channel, m
Pr = Prandtl number, $c_p\mu/k_l$
p = pressure, N/m²
Re = Reynolds number, $\rho du/\mu$
T = temperature, °C
t = time, s
u = velocity, m/s
v = specific volume, m³/kg
v_{fg} = $v_g - v_f$
We = Weber number
z = axial coordinate, m
α = volume fraction
δ = vapor film thickness, m
ε = emissivity
η_e = volume fraction of entrainable drops
μ = viscosity, kg/ms
σ = surface tension
σ_r = Stefan-Boltzmann constant
τ''' = shear force per unit volume, N/m³

Subscripts
c = convection
conv = convection
d = droplet
evap = evaporation
i = vapor-liquid interface
j = axial node
l = liquid
lH = liquid heating
rad = radiation
sat = saturation
v = vapor
w = wall

Superscripts
$''$ = quantity per unit area
$'''$ = quantity per unit volume
r = radiation

Received April 21, 1992; revision received Aug. 7, 1992; accepted for publication Aug. 10, 1992.

*Senior Engineer; currently Advance Program Development and Production Support, McDonnell Douglas Space Systems, 689 Discovery Drive, Huntsville, AL 35806. Member AIAA.
†Professor of Engineering Science and Mechanics. Member AIAA.
‡Department of Chemical Engineering and Applied Chemistry.

Introduction

IN the future, cryogenic refueling of space-based transport vehicles and satellites will constitute an essential operation for long-term space missions. To achieve optimum flow rates

in the process of refueling, the temperature of the transfer line must be lowered to a point at which the fluid passing through remains in the liquid phase. In order to design and operate the transfer lines and storage systems, parameters such as the duration of cool-down and the amount of the coolant must be known. To attain this objective, a comprehensive study of the cool-down process (both in 1 *g* and in microgravity) are undertaken. The present work deals with 1-*g* conditions only. The work discussed in this article comprises an initial stage of a long-term research directed toward understanding the larger problem of the transfer line chill-down in the low-gravity environment of space. The main focus here is on developing reliable predictive tools in 1 *g* conditions, which can then be extended to low gravity conditions for the process of cooling down a transfer line.

When cryogenic liquid enters a hot tube, the cool-down process commences with the production of simultaneous vapor and two-phase liquid-vapor flow, leading to the desired reduction of the line temperature. This process continues until the line temperature reaches the saturation temperature of the liquid. The specific two-phase flow pattern through which this condition is achieved depends on several critical parameters. Principal among those, are the tube orientation and the cooling liquid temperature and flow rate. Keeping in mind the original requirement of extending the present analysis to a low-gravity environment, vertical tube orientation is considered here. For the bottom reflood of a vertical tube, Kawaji et al.[1] performed a series of experiments aimed at understanding the flow patterns arising when a cold liquid enters a hot tube. They found two principal sequences of flow patterns occurring, depending on whether the liquid is subcooled or at saturation conditions, and also whether the liquid injection rate is high or low. In the bottom reflood, the entering liquid will initially boil through the film boiling mechanism for the fast flow case, and through saturated boiling in the slow flow case, developing into annular flow in the latter and inverted annular flow in the former. In both cases, the flow subsequently develops into a dispersed flow pattern in which the droplets eventually evaporate leading to fully vapor flow.

There have been several early studies concerning the different aspects of the line cool-down problem.[2–7] All of these studies are mainly empirical in nature which cannot easily be extended to new conditions for which no data exist, such as a low-gravity environment. Recent efforts in two-phase, liquid-vapor thermohydraulic modeling have concentrated on exploiting the multifield model. A two-fluid version of such a model was used successfully for predicting the refilling and rewetting of a horizontal tube by Chan and Banerjee.[8,9] Kawaji and Banerjee[10,11] also employed the two-fluid model to predict the thermohydraulic criteria for the bottom reflood problem. Their results agreed reasonably well with experimental data obtained for the steam-water system. In the present work, the two-fluid model developed by Kawaji and Banerjee is used to predict the chill-down mechanism in a vertical tube by injecting liquid nitrogen. Such models may be extended to variable gravity conditions if the flow pattern is well understood.

Two-Phase Flow Model

One of the relevant input data needed for implementing the two-fluid flow models is the knowledge of the correct sequence of flow patterns arising during the two-phase flow process. Thus, the first task in the present transfer line chill-down modeling effort is comprised of establishing this data base. To achieve this objective, a cryogen chill-down experiment was designed and constructed. The test section was constructed of a copper tube 12.7 mm o.d., and approximately 366-cm long. The tube was insulated and held vertically and was kept at room temperature with its upper end open to the atmosphere. The working fluid was liquid nitrogen whose flow was monitored with a cryogen flow meter. The test section was instrumented with thermocouples positioned in pairs at approximately 30-cm intervals along the axial direction on the outside surface of the tube. Each element of the thermocouple pair was placed on opposite sites of the circumference of the tube. A pressure gauge was placed close to the entrance of the test section as well as several thermocouples placed at selected locations along the flow loop. Figure 1 shows a schematic of the flow loop adopted for the experiment. Full details of the experiment, instrumentation, and operation of the tests performed are given by McGee.[12]

The experiment was run for several liquid expulsion pressures representing different flow rates in the test section of the liquid nitrogen coolant. The expulsion pressure is that pressurization pressure applied at the LN2 dewar to force the flow of LN2 into the test section. For each test run, all of the thermocouple outputs were recorded, as well as the response of the pressure gauges and the flow meter signals. Figure 2 shows the temperature history, $T = T(t)$ of five thermocouples at different axial locations along the test section. The figure shows the temperature response for only one of the pair of thermocouples at each location since every pair gave essentially identical temperature response. The conditions for the run shown in Fig. 2 are for liquid nitrogen expulsion pressure of 34.5 kN/m^2 (5 psig) representing a flow rate of 29.2 cm/s.

Based on the shape of the cooling curves shown in Fig. 2 and also from the experiments of Ganic and Rohsenow[13] and Laverty and Rohsenow,[14] it was concluded that the two-phase liquid-vapor flow in the test section during quench was basically composed of the following four patterns. Below the quench front the flow is made up of "fully liquid" with some nucleate boiling taking place at the tube wall. As the liquid

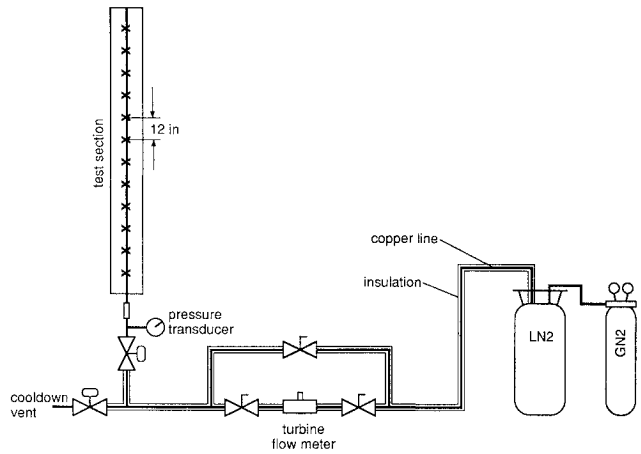

Fig. 1 Schematic for the flow loop for the liquid nitrogen chill-down experiment.

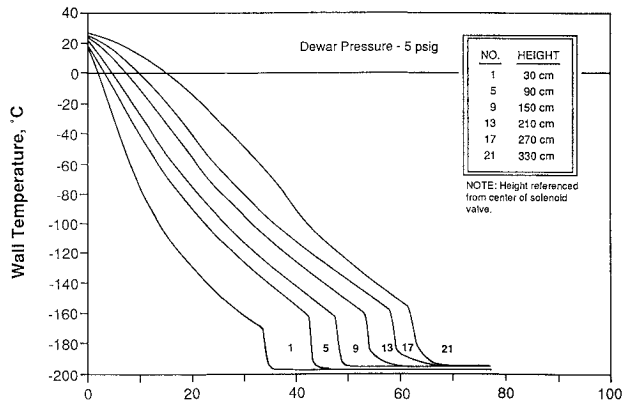

Fig. 2 Temperature histories at several axial locations along the test section of the liquid nitrogen chill-down experiment for an expulsion pressure of 34.5 kN/m^2.

is heated by the wall, liquid boiling will commence leading to an "inverted annular flow" regime comprised of a liquid core surrounded by a vapor film next to the tube wall, immediately downstream of the quench front. This liquid core will then break up into filaments and droplets leading to a "dispersed flow" regime. The liquid droplets will then vaporize as they are carried by the vapor along the tube resulting in a "fully vapor" region far enough from the quench front. In separate experiments on quenching with liquid nitrogen, Laverty and Rohsenow[14] concluded (based on photographic evidence) that the boiling flow patterns recorded in their quartz tube were basically similar to the those described here. In later experiments on liquid nitrogen, Ganic and Rohsenow[13] obtained tube wall temperature histories (their Fig. 3) that are very similar to the curves shown here in Fig. 2. The quench flow patterns that are being modeled were defined based on the evidence from our experiments and these studies.

Mathematical Model

The most challenging aspect of the mathematical formulation in the present model is the correct prediction of the thermohydraulic characteristics of the two-phase flow regions, namely the inverted annular and the dispersed flow regimes. At present, a highly robust model for two-phase flow may be obtained through the two-fluid formulation. The details of such formulation are thoroughly reviewed by Ishii.[15] Basically, this method describes each phase (i.e., liquid and vapor) by its proper conservation equations with the appropriate constitutive (matching) laws at the interfaces of the two phases.

The sequence of flow patterns arising from the chill-down experiments discussed in the previous section is very similar to the flow patterns employed by Kawaji and Banerjee[10,11] for their model for the "loss of coolant accident" analysis. The two-fluid, liquid-vapor mathematical model adopted here for the line chill-down experiment will be analogous to the one used by Kawaji and Banerjee.[11] The model adopted for this study will use the same conservation equations for each phase as in Kawaji and Banerjee,[10,11] except in here the physical properties of liquid/vapor nitrogen will be used instead of water/steam. Also, some of the constitutive relations used in this study to close the model are different, since whenever possible the appropriate empirical formulas for cryogenic conditions are used. Therefore, a two-fluid model with four distinct regions, namely 1) fully liquid, 2) inverted annular flow, 3) dispersed flow, and 4) fully vapor, is considered for describing the flowfield. In addition, a one-dimensional energy equation is formulated for predicting the temperature history of the tube wall.

Inverted Annular Flow Region

For the inverted annular flow region it is assumed that the flow is made up of a liquid column which is surrounded by a vapor film. In the present model, the shape of either the liquid core or the vapor film is assumed to be a function only of the axial direction z in which the vapor film thickness is designated by $\delta(z)$. A sketch of the physical interpretation of the inverted annular flow model is shown in Fig. 3a.

The mathematical description of this region is obtained through the conservation equations for each of the liquid core and the surrounding vapor film (i.e., the two-fluid model). The area-averaged equations of motion result in the one-dimensional, two-phase flow equations for the inverted annular flow regime which take the following form:

Liquid mass

$$\frac{\partial}{\partial t}(\alpha\rho)_l + \frac{\partial}{\partial z}(\alpha\rho u)_l = -m_l''' \tag{1}$$

Vapor mass

$$\frac{\partial}{\partial t}(\alpha\rho)_v + \frac{\partial}{\partial z}(\alpha\rho u)_v = m_l''' \tag{2}$$

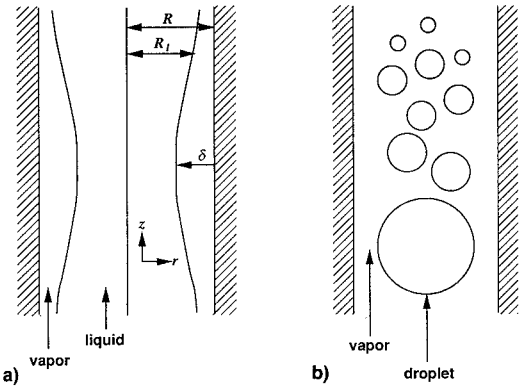

Fig. 3 Sketch for the physical model adopted in the numerical computations for a) the inverted annular flow regime and b) the dispersed flow regime.

Liquid momentum

$$\frac{\partial}{\partial t}(\alpha\rho u)_l + \frac{\partial}{\partial z}(\alpha\rho u u)_l + \alpha_l \frac{\partial p_l}{\partial z} - \Delta p_{li}\frac{\partial \alpha_l}{\partial z} = \tau_i''' - \rho_l \alpha_l g - m_l''' u_i \tag{3}$$

Vapor momentum

$$\frac{\partial}{\partial t}(\alpha\rho u)_v + \frac{\partial}{\partial z}(\alpha\rho u u)_v + \alpha_v \frac{\partial p_v}{\partial z} - \Delta p_{vi}\frac{\partial \alpha_v}{\partial z} = -\tau_i''' - \rho_v \alpha_v g + m_l''' u_i - \tau_{wv}''' \tag{4}$$

Liquid energy

$$\frac{\partial}{\partial t}(\alpha\rho h)_l + \frac{\partial}{\partial z}(\alpha\rho u h)_l = -m_l''' h_{l,\mathrm{sat}} + q_{lI}''' \tag{5}$$

Vapor energy

$$\frac{\partial}{\partial t}(\alpha\rho h)_v + \frac{\partial}{\partial z}(\alpha\rho u h)_v = m_l''' h_{v,\mathrm{sat}} + q_v''' \tag{6}$$

These equations were derived based on the assumption that the average of products of the dependent variables is equal to the product of the averages. The terms Δp_{li} and Δp_{vi} are the pressure difference between the liquid interface and the liquid phase or the vapor phase, respectively. Details of the derivation of the above equations are given in Banerjee and Chan.[16] These systems of equations can be applied to any two-phase flow pattern once the proper constitutive models for the heat flux and shear stress for each flow regime and across all interfaces are properly defined.

Equations (1–6) can be solved only when all of the shear stress and heat and mass flux terms appearing on the right sides of the equations are given in terms of the dependent variables. Normally, these expressions are empirical in nature and can only be known from experimentation. Depending on the specific flow regime, these functions can be obtained from laborious and detailed experiments. The specific empirical formulas used in the present analysis for m_l''', τ_i''', τ_{wv}''', q_{lH}''', and q_v''' are given in Table 1. Also, Table 1 identifies the source of these formulas.

Dispersed Flow Region

Instabilities of the interfacial waves (which exist at the vapor-liquid interface) in the inverted annular flow regime have been reported by Forslund and Rohsenow,[17] Lee and Ryley[18] and Kawaji and Banerjee.[10] These instabilities normally lead to the transition from inverted annular to dispersed flow region. In the present model, it is assumed that once liquid

Table 1 Constitutive relationships for inverted annular film boiling flow

Description	Equation	Reference
Heat flux to vapor	$q''_v = q''_{wv} + q''_{vl}$	
Heat flux wall-to-vapor	$q''_{wv} = (k_v Nu_t/2\delta)(Tw - Tv)$	25
Heat flux vapor-to-liquid	$q''_{vl} = (k_v Nu_0/2\delta)(T_v - T_l)$	25
Vapor film thickness	$\delta = R(1 - \sqrt{\alpha_l})$	
Heat per unit volume	$q''' = (4/d)q''$	
Liquid heat flux	$q''_l = q''_{vl} + q''_{\text{rad}} = q''_{lH} + q''_{\text{evap}}$	
Radiative heat flux wall-to-liquid column	$q''_{\text{rad}} = \dfrac{\sigma_r(T_w^4 - T_{\text{sat}}^4)}{(1/\varepsilon_w) + (1/\varepsilon_l\sqrt{\alpha_l}) - 1}$	
Vaporization rate per unit volume	$m'''_l = q'''_{\text{evap}}/L_{fg}$	
Wall heat flux	$q''_w = q''_{\text{rad}} + q''_{wv}$	
Wall-to-vapor shear stress: Laminar	$\tau'''_{wv} = \dfrac{16\mu_v}{d^2}\left\{\dfrac{-u_l/2\xi + u_v(2\xi + \alpha_v)}{\alpha_v + (1 + \alpha_l)\xi} + \dfrac{u_l[1 + 2\alpha_l\xi/\alpha_v + \alpha_l + \alpha_v/(2\xi)]}{\alpha_v + (1 + \alpha_l)\xi}\right\}$	10
	$\xi = m\sqrt{\alpha_l}$	
Turbulent	$\tau'''_{wv} = 2(f_w/d)\,\rho_v\lvert u_v\rvert u_v$	
	$f_w = \left(\dfrac{0.085}{Re^{0.25}}\right), \quad Re = (\rho_v\lvert u_v\rvert 2\delta/\mu_v)$	
Liquid-vapor interfacial Shear stress:		
Laminar	$\tau'''_i = \dfrac{16\mu_v}{d^2}\left\{\dfrac{u_l/2\xi = u_v(2\xi\alpha_l + \alpha_v)}{\alpha_v + (1 + \alpha_l\xi)} + \dfrac{u_l[2\alpha_l + 2\alpha_l\xi/\alpha_v + \alpha_v/(2\xi)]}{\alpha_v + (1 + \alpha_l\xi)}\right\}$	10
Turbulent	$\tau'''_i = (2\alpha_l^{0.5}/d)f_i\rho_v\lvert u_v - u_l\rvert(u_v - u_l)$	
	$f_i = (0.085/Re^{0.25}), \quad Re = [\rho_v\lvert u_v - u_l\rvert 2\delta)/\mu_v]$	

detachment has been detected, the detached liquid chunks break up into a population of droplets. The second two-phase flow regime used in this model is the dispersed flow. The flowfield in this region consists of liquid drops embedded in a vapor background. It is assumed for this problem that droplets of various sizes are generated at the top of the inverted annular flow regime as the liquid column disintegrates. The drop sizes will change as the liquid evaporates during their entrainment up the tube. Assuming the liquid drops to be perfect spheres, the most critical parameter in this region is the drop size distribution. The subsequent energy transport depends strongly on the entrained droplet size distribution. A sketch of the physical model used for the dispersed flow region is shown in Fig. 3b. Again, for this regime a two-fluid model is used to describe the flow, one for the droplets and another for the vapor phase.

Assuming the vapor and the liquid pressures to be uniform and equal to the tube exit pressure, and the droplets to be perfect spheres with a given size distribution function, the conservation equations take the following form:

Drop mass

$$\frac{\partial}{\partial t}(\alpha_l\rho_l) + \frac{\partial}{\partial z}(\eta_l\alpha_l\rho_l u_d) = -m'''_l \tag{7}$$

Vapor mass

$$\frac{\partial}{\partial t}(\alpha_v\rho_v) + \frac{\partial}{\partial z}(\alpha_v\rho_v u_v) = m'''_l \tag{8}$$

Drop momentum

$$\frac{\partial}{\partial t}(\eta_l\alpha_l\rho u_d) + \frac{\partial}{\partial z}(\eta_l\alpha_l\rho_l u_d u_d) = \tau'''_d - \eta_l\alpha_l\rho_l g - \eta_l m'''_l u_d \tag{9}$$

Drop energy

$$\frac{\partial}{\partial t}(\alpha_l\rho_l h_d) + \frac{\partial}{\partial z}(\eta_l\alpha_l\rho_l u_d h_l) = -m'''_l h_{l,\text{sat}} + q'''_{dH} \tag{10}$$

Vapor energy

$$\frac{\partial}{\partial t}(\alpha_v\rho_v h_v) + \frac{\partial}{\partial z}(\alpha_v\rho_v u_v h_v) = m'''_l h_{l,\text{sat}} + q'''_v \tag{11}$$

It should be noted here that the vapor momentum equation is neither used nor listed for the dispersed flow region. The reason for this omission is that the vapor pressure in the dispersed flow region is taken to be the ambient pressure, since the model assumes the exit of the tube to be open to the atmosphere. Thus, vapor pressure is not an unknown of the problem, making the vapor momentum equation unnecessary.

The primary variables for this case are the same as for the inverted annular flow regime, namely: α, ρ, u, and h. Again, the terms τ'''_d, η_l, m'''_l, q'''_{dH}, and q'''_v are calculated from appro-

Table 2 Constitutive relationships for dispersed flow

Description	Equation	Reference
Heat flux wall-to-vapor	$q''_{wv} = 0.023\left(\frac{k_f}{d}\right) Re^{0.8}Pr^{0.33}(T_w - T_v)$	13
Radiative heat flux among wall, vapor, and drops	$q''^{r}_{ij} = F_{ij}\sigma_r(T_i^4 - T_j^4)$	26
	ij represents either wd (wall-to-drop), wv (wall-to-vapor), or vd (vapor-to-drop)	
	$F_{vd} = (R_v + R_d + R_vR_d/R_w)^{-1}$	
Wall-drop interaction heat transfer	$q''_{wd} = A(T_w - T_{sat})^{0.75}(D_v/D_{smd})$	17
	$A = 0.2552\left[\frac{k_f^3 L^*_{fg} g\rho_v\rho_l}{\mu_v D_v}\right]^{0.25}\alpha_l^{2/3}$	
	$L^*_{fg} = L_{fg}[1 + \frac{7}{20}c_p(T_w - T_{sat})/L_{fg}]^{-3}$	
Vapor-to-drop convective heat transfer	$q''_{vd} = (k_f/D_a)(2 + 0.74Re_d^{0.5}Pr_f^{0.33})(T_v - T_d)$	18
	$Re_d = \rho_v\lvert u_v - u_l\rvert D_a/\mu_v$	
Heat flux to vapor	$q''_v = q''_{wv} + q''^{r}_{wv} - q''^{r}_{vd} - q''_{vd}$	
Heat flux to droplets	$q''_d = q''_{vd} + q''^{r}_{vd} + q''_{wd} + q''^{r}_{vd}$	
	$q''_d = q''_{evap} + q''_{dH}$	
Evaporation rate per unit volume	$M'''_l = q'''_{evap}/L_{fg}$	
Wall heat flux	$q''_w = q''_{wv} + q''^{r}_{wv} + q''^{r}_{wd} + q''_{wd}$	
Drag force on a particle	$\tau'''_d = (18\alpha_l D_a^2/D_v^3 Re_d)(\rho_v - \rho_l)\lvert u_v - u_l\rvert(1 + 0.15Re_d^{0.687})$	27

priate constitutive models which are incorporated into the equation system. The constitutive relations used for these terms and their sources for the dispersed flow region are shown in Table 2. It should be noted that the dispersed flow model can also be used to describe the fully vapor region by allowing the droplet diameter to shrink to zero.

Single-Phase Fluid Flow Region

The chill-down model adopted in this investigation considers two single fluid flow regions, in addition to the two-phase flow regions discussed above. The first is the fully liquid region immediately below the quench front, and the other is the fully vapor region above the dispersed flow region. Since a one-dimensional flow model is being adopted here, the fluid velocity in either of the single fluid regions is described by very simple relations. However, the heat flux in both the axial and the radial directions requires some attention.

The heat transfer mechanism in the fully liquid and the fully vapor regions is basically the wall-to-fluid forced convection. For a constant density, fully developed one-dimensional flow the conservation equations for the liquid phase are as follows:

Continuity

$$\frac{\partial u_l}{\partial t} = 0 \tag{12}$$

Energy

$$\rho_l\frac{\partial h_l}{\partial t} + \rho_l u_l\frac{\partial h_l}{\partial z} = 4\frac{q''_w}{d} \tag{13}$$

where the local wall heat flux is given by

$$q''_w = h_c(T_w - T_l) \tag{14}$$

Close to the quench front, if the channel wall temperature is sufficiently higher than the liquid saturation temperature, the heat flux increases due to nucleate boiling. To determine the position of the boiling incipience in a flow channel, Papell and Hendricks[19] suggested a correlation equation for boiling incipience, which was solved iteratively. Bergles and Rohsenow[20] developed a different criterion for the onset of nucleate boiling of water. For cryogenic liquid, that criterion was modified by Frost and Dackowic[21] as follows:

$$(T_w - T_{sat}) = [(4B/k_l)q''_w]^{0.5}Pr \tag{15}$$

$$B = (2\sigma T_{sat}v_{fg}/L_{fg}) \tag{16}$$

The total heat flux is the sum of forced convection and nucleate boiling. For cryogenic liquids, Girratano et al.[22] suggested the following correlation:

$$h_{total} = h_{nb} + h_c \tag{17}$$

where

$$h_{nb} = 0.487(10)^{-10}\left[\frac{k_l\rho_l^{1.282}p^{1.75}c_{pl}^{1.5}}{(L_{fg}\rho_v)^{1.5}\sigma^{0.906}\mu_l^{0.626}}\right]\Delta T^{1.5} \tag{18}$$

$$h_c = 0.023Re_l^{0.8}Pr_l^{0.4}(k_l/d) \tag{19}$$

For the fully vapor region, on the other hand, the heat flux is only due to the forced convection of the vapor past the tube wall. In the present model, however, this region is solved using the dispersed flow model with zero droplet size.

Tube Wall Region

The model adopted here considers a finite-thickness tube wall through which axial conduction occurs. However, the

tube wall is taken to be very thin such that the radial conduction across the tube wall is negligible. The one-dimensional energy equation for the tube wall is given by

$$\rho_w c_{pw} \frac{\partial T_w}{\partial t} = \frac{\partial}{\partial z}\left(k_w \frac{\partial T_w}{\partial z}\right) - \frac{P_i}{A_w} q''_w \tag{20}$$

The value of q''_w depends on the specific flow regime, whether two-phase or single-phase and on the specific fluid.

Numerical Solution

The numerical method employed here follows along the same lines developed by Kawaji and Banerjee[11] for their solution for the bottom reflood problem. The entire model is solved by means of the finite-difference method using both the implicit and the explicit formulations. First, the domain of solution including the interior of the tube and the tube wall is subdivided into a number of computational elements. In this case, since the geometry is one-dimensional, each node extends from one wall to the other in the radial direction with the node numbers increasing in the axial direction from the lower end of the tube to the top. Two mesh sizes are adopted in the calculations for this article, one for the inverted annular flow and wall regions and another for the dispersed flow and fully vapor flow regions. The specific node sizes used will be discussed in the next section.

In order to calculate the wall temperature at each node and at every time step, the local wall heat flux must be known from the flow and heat transfer computations. Flowfield and heat transfer calculations are performed at each node at every time step. After specifying the input parameters and initializing the dependent variables, the computations begin with the inverted annular flow regime. The lower boundary of this region is always fixed at the quench front whose location at all times is a prescribed input data. An implicit finite-difference scheme is used for this region. Liquid density, in this region, is assumed a constant, while the vapor density is a function of temperature. Using the liquid mass conservation equation, the liquid and vapor fractions are first computed. Next, the vapor energy and continuity equations are solved for the vapor temperature. The vapor density and velocity can then be determined. The vapor momentum equation is subsequently used to determine the vapor pressure throughout this region. Since this problem is solved with the upper end of the tube open to the atmosphere, the vapor pressure at the top of the inverted annular region is assumed to be equal to the background pressure, the atmospheric pressure in the present case. This assumption requires that the vapor pressure calculations be started from the uppermost node of the inverted annular regime. Proceeding downwards to the quench front, the vapor pressure is determined. Using the liquid momentum equation, the liquid velocity is calculated next. The equations discussed above are solved iteratively at each time step until agreement between the calculated liquid velocity below the quench front and the prescribed liquid inlet velocity are matched. This is the implicit portion of the solution procedure. The convergence of the computations in this region is fast whenever values from the previous time step are used. In the present case only two or three iterations are sufficient for most calculations. Once convergence is obtained, the liquid energy equation is solved explicitly to determine the liquid temperature. All of the computational details employed in this problem including those discussed above can be found in Hedayatpour.[23]

Having evaluated all of the fluid properties for the inverted annular flow region, including the phasic fractions, the height of this region is then established. It is assumed that as the liquid surface waves are sufficiently amplified, necking of the liquid column occurs which determines the inverted annular/dispersed flow regime boundary. The following criteria which was also used by Kawaji and Banerjee[10] is employed in here to determine the necking condition for the liquid column:

$$\alpha_{lj} < 0.5 \tag{21a}$$

or

$$[(\alpha_{lj-1} - \alpha_{lj})/\Delta z] > 0.15 \tag{21b}$$

$$\alpha_{lj+1} > 0.6 \tag{21c}$$

The subscript j indicates the nodal number.

The next segment in the computational procedure is to evalaute the flow variables for the dispersed flow region whose lower boundary is already known by the procedure outlined above. These variables are determined through the numerical solution of Eqs. (7–11). The explicit finite-difference technique is employed for solving these equations. An essential parameter in this region is the liquid drop size distribution. Again, the drop distributions employed by Kawaji and Banerjee[11] are used here to produce the results discussed in the next section. In the present analysis a transition region between the inverted annular and the dispersed flow regions was also included in the model. In the transition region the liquid drops are expected to exist in larger sizes than in the fully dispersed flow region. Since the necking criteria used in the inverted annular region allows the breakup of liquid columns of lengths up to 4.5 times the liquid jet diameter, the liquid drops in the transition region were considered to be ellipsoidal in shape with a minor semiaxis of the order of the tube radius. In order to incorporate such large drop sizes, the value of one of the size distribution parameters was modified to allow for the flow transition regime.

At a given elevation, the actual size distribution is cut off at a maximum diameter $D_{\max}$ which is equal to either the smaller of the maximum stable diameter at that elevation $D^s_{\max}$, or the maximum entrainable diameter $D^e_{\max}$. $D^s_{\max}$ is determined from a balance between the vapor inertial force and the surface tension force characterized by We in the following manner:

$$D^s_{\max} = \sigma(We_c/\rho_v u_v^2) \tag{22}$$

Forslund and Rohsenow,[17] Hinze,[24] and Kawaji and Banerjee[10] have all reported different values for We_c, ranging from 6 to 22. In the calculations discussed below, a range of values of We_c was used, but the results indicated no observable dependence of the main variables on the value used. In the present work a value of We_c of 15 is used. The maximum size of entrainable droplet diameter is found from a balance between the gravity and the drag forces on the droplet:

$$D^e_{\max} = (18/Re_d)\,(1 + 0.15Re_d^{0.687})[\rho_v u_v^2/g(\rho_l - \rho_v)] \tag{23}$$

The liquid momentum equation in the present model describes the motion of the drops carried upward by the vapor. The carryover fraction is calculated from the ratios of the integrals of the size distribution functions.

The numerical solution in the dispersed flow region is accomplished by first explicitly finite-differencing the drop continuity equation [Eq. (17)] to determine the liquid and void fractions for the new time step. Next the vapor continuity and energy equations [Eqs. (8) and (11)], are finite-differenced together to determine the vapor temperature. Once the vapor temperature at the new time step is known, the vapor density can be calculated and the vapor velocity is determined from the vapor continuity equation. Finally, the drop momentum and energy equations [Eqs. (9) and (10)], are explicitly finite-

differenced to determine both the drop velocity and the drop temperature.

Results and Discussion

The first step in the computational procedure adopted here is to define the various computational meshes needed. The following three sizes of nodes are used for the calculations discussed below: 1) fluid-dynamic nodes applicable for the inverted annular flow and the fully liquid regions each 2.5-cm long; 2) fluid-dynamic nodes in the dispersed flow region each 33-cm long; and 3) heat conduction nodes in the tube wall each 2.5-cm long. Since the finite-differencing scheme adopted in the calculations is comprised of a mixed implicit and explicit techniques, the time step for such a system is normally governed by the explicit stability criteria. The time step size Δt used throughout the computations is fixed such that the Courant stability criterion

$$(u_{\max}\Delta t/\Delta z) < 1 \tag{24}$$

is always satisfied for each computational node.

As already discussed, the principal objective of the numerical procedure described in the previous section is to predict the quench characteristics in the tube for the vertical flooding experiment described above. Basically, it is attempted here to validate the code through checking against the pertinent physical characteristics of the experiment. A code for the cool-down process based upon the model described in the previous section was developed and validated for liquid nitrogen as the working fluid. In addition to the necessary initial and boundary conditions, the code also requires as input data the quench front time history for the specific experiment. Figure 4 shows several experimental quench front histories for the tests described earlier. For the numerical simulations of each experiment the appropriate data curve in Fig. 4 is used. The data for the test section geometry and material were also incorporated into the code. Specifically, the test section for the experiments to be validated here was a copper tube of 12.7-mm o.d. and 366-cm long with 1.6-mm wall thickness insulated with 7.5-cm thick insulation along the length of the tube, and whose temperature was initially set to room conditions. Liquid nitrogen at saturation temperature was injected into the tube by pressurizing the liquid nitrogen dewar and opening the inlet valve at the lower end of the test section. Using the quench front characteristics from the experiment as shown in Fig. 4, the wall temperature history for different elevations was then calculated. The code commences the computations at the instant the valve located just upstream of the entrance to the test section is opened. Implied in this procedure is that at that time, or shortly thereafter, only liquid nitrogen is being admitted at the inlet of the test section.

The 12.7-mm-o.d. tube used for both the computations and the validation experiments was chosen in order to compare the results with previous studies. Both Laverty and Rohsenow[14] and Ganic and Rohsenow[13] used 13-mm-o.d. nominal tubes in their liquid nitrogen boiling experiments. Also, Kawaji and Banerjee[10,11] used a 14-mm-o.d. tube in their reflooding experiments and also in their model. For these reasons it was decided that by using a 12.7-mm-o.d. tube for the test section, a direct comparison could be made conveniently with both previous experiments and previous numerical modeling efforts.

Initial validations of the model described above did not yield acceptable predictions for the tube wall temperature histories. The reason being that the assumption of the existence of a fully liquid region at the entrance to the test section immediately after the valve is opened could not be justified from the experimental configuration. Examination of the experimental temperature histories of Fig. 2 reveal that a relatively long time elapses before the 30-cm location is quenched. Also, inspection of the apparatus shows that the valve that allows the liquid coolant to enter the test section is not actually situated at the test section entrance. Furthermore, that same valve will normally have a finite thermal mass which can supply energy to the liquid coolant. Such energy transfer could cause the liquid to immediately vaporize until the valve temperature drops close to the saturation temperature of the coolant. For these reasons the code was slightly modified in order to account for both the inlet valve and the tubing section upstream of the test section.

Figure 5 shows the calculated and the measured temperature histories at the outer wall of the test section tube for a coolant injection rate of 29.2 cm/s. Initially, for the first 30 s of the run, in this case, all of the liquid entering the test section was allowed to evaporate in the numerical model. Subsequently, the two-phase flow model is initiated with the exact sequences as described in the previous section. The initial evaporation period of 30 s was chosen from the quench front histories of Fig. 4. It is seen that for the 34.5 kN/m^2 test run the extension of the quench front speed curve intersects the abscissa at about the 30-s mark. It can be seen from Fig. 5 that there is excellent agreement between the calculated temperature history and the measured data.

Figure 6 shows the calculated and the measured temperature histories for the same conditions as in Fig. 5 at two additional axial locations of 90 and 150 cm, respectively, downstream of the inlet to the test section. This figure shows that a reasonably close agreement exists between the numerical model and the measured experimental data. However, it is clear that the experimental data was never exactly reproduced with the two-phase flow model adopted in this study. Figure 6 shows that the calculated temperatures are higher for the lower locations and lower at the higher locations than the measured temperatures.

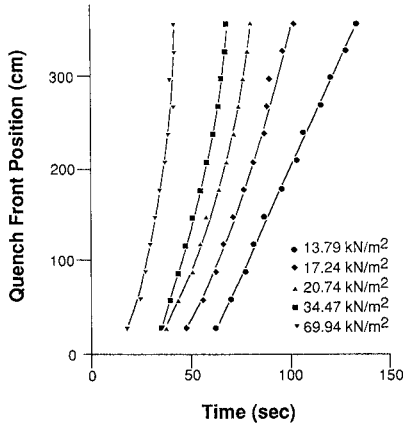

Fig. 4 Experimental quench front histories for flows at different expulsion pressures.

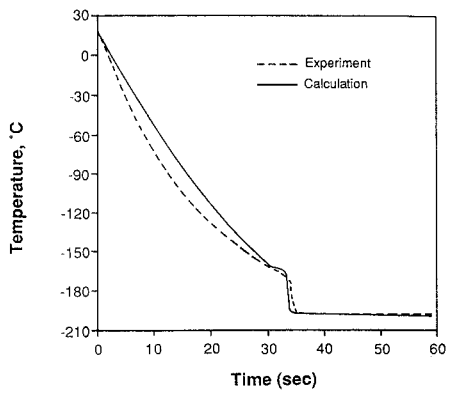

Fig. 5 Calculated and measured temperature histories at the 30 cm axial location for 34.5 kN/m^2 expulsion pressure.

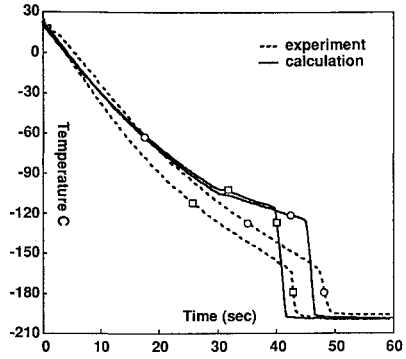

Fig. 6 Calculated and measured temperature histories at two axial locations for 34.5 kN/m² expulsion pressure: -◇-, at 90 cm from the inlet to the test section, and -○-, at 150 cm from the inlet.

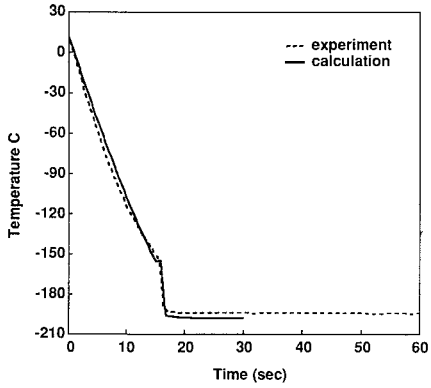

Fig. 7 Calculated and measured temperature histories at the 30-cm location from the inlet to the test section for 69 kN/m² expulsion pressure.

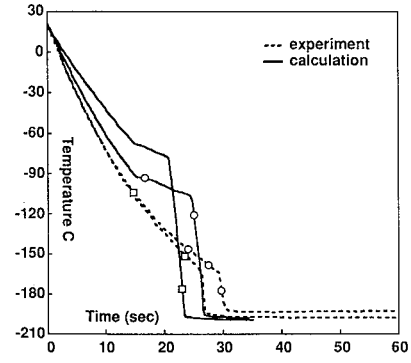

Fig. 8 Calculated and measured temperature histories at two axial locations for 69 kN/m² expulsion pressure: -◇-, at 90 cm from the inlet to the test section, and -○-, at 150 cm from the inlet.

Figure 7 shows the calculated and measured temperature time histories at the 30-cm locations from the inlet to the test section for a liquid nitrogen expulsion pressure of 69 kN/m². Figure 8 shows the temperature histories again at the 90 and 150 cm locations, respectively, from the test section entrance for an expulsion pressure of 69 kN/m². Figure 9 shows the calculated and measured temperature time histories at the 30-cm locations from the inlet to the test section for a liquid nitrogen expulsion pressure 20.7 kN/m². Figure 10 shows the temperature histories again at the 90 and 150 cm locations, respectively, from the test section entrance for an expulsion pressure of 20.7 kN/m². The calculations of Figs. 7–10 were produced using the same model as in Figs. 5 and 6 in which the liquid was allowed to evaporate at the commencement of the test for a specified time period. However, the evaporation period allowed in each calculation varied from case to case.

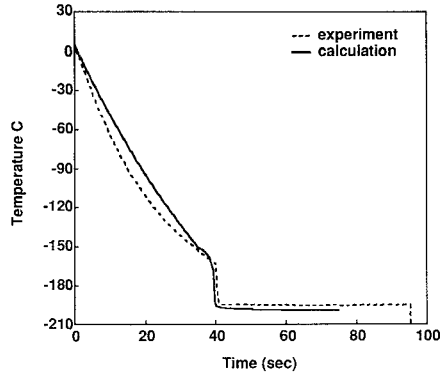

Fig. 9 Calculated and measured temperature histories at the 30-cm location from the inlet to the test section for 20.7 kN/m² expulsion pressure.

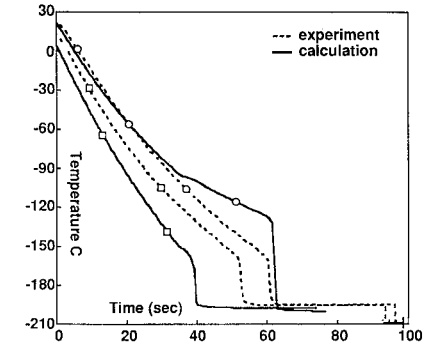

Fig. 10 Calculated and measured temperature histories at two axial locations for 20.7 kN/m² expulsion pressure: -◇-, at 90 cm from the inlet to the test section, and -○-, at 150 cm from the inlet.

The evaporation period for each case was calculated according to Fig. 4 for the appropriate expulsion pressure, in which case its value was determined from the intersection of the extension of each curve with the abscissa. The evaporation period for the 69 kN/m² pressurization (Figs. 7 and 8) was determined to be 15 s, while for the 20.7 kN/m² case (Figs. 9 and 10) it was 35 s.

By observing the wall temperature histories of the experimental data and the results of the model, it could be seen that the calculated values are underpredicted, which means that the energy fluxes are overpredicted. At the higher elevations of the test section the predicted wall temperature decreases faster than the measured wall temperature. Tube wall overcooling could be due to reduction of the superheated vapor temperature for the following reasons. By leaving the inverted annular flow region, superheated vapor loses much of its sensible heat to drops by convective heat transfer from the wall, and this heat transfer is overpredicted further downstream where the velocity, convective heat transfer coefficient, and the difference between the wall and vapor temperatures become relatively large due to drop vaporization in the upstream region. Also, convective heat transfer from superheated vapor to drops may have been overpredicted due to high heat transfer coefficient because an equilibrium size distribution was used to calculate droplet size which may be different than the actual distribution.

The results of the calculations shown in Figs. 5–10 appear to agree well with the experimental results. However, this agreement is to be viewed with caution since an essential data input into the code is an experimental result, namely the quench front speed. A quench front speed could have been assumed as a function of the coolant and the tube thermal properties, as well as the coolant injection rate. Another assumption which must be addressed if this code is to be used in a different application, is the quench flow pattern. As indicated, the quench flow pattern modeled here was assumed

based on the tube wall temperature history, and not based on the actual experimentally observed pattern in this case. The agreement between the calculations and the experiment could possibly have been better had the exact flow pattern been known. Nevertheless, reasonably accurate results were calculated in spite of these drawbacks, indicating that the two-fluid model is quite robust and useful in many applications.

Conclusions

Based on the flow patterns obtained in past studies and the present experimental observations, a two-phase flow model with the following flow regions was developed: 1) fully liquid, 2) inverted annular film boiling, 3) dispersed flow film boiling, and 4) fully vapor. A transient two-fluid model was developed to describe the two-phase flow regions. A set of mass, momentum, and energy equations was solved for each phase with the necessary constitutive relations describing the wall-to-fluid interfacial transport of the mass, momentum, and energy. The liquid injection rate into the test section was considered to be constant. To compute the wall temperature, a one-dimensional energy equation was formulated. For the inverted annular flow regime, a set of six fully transient conservation equations were solved. In the present model, the phases were assumed to be completely separated with liquid flowing in the center of the flow channel. Heat transfer mechanisms for this region were as follows: 1) wall-to-vapor convection, 2) wall to liquid radiation, and 3) vapor-to-liquid convection.

For the dispersed flow regime, a two-fluid model consisting of five transient conservation equations was considered. To model the drop size distribution, an upper-limit, log-normal distribution function was assumed. In this region the following heat transfer mechanisms were considered: 1) wall-to-vapor convection; 2) wall-drop interaction; 3) vapor-to-drop convection; and 4) radiation among wall, vapor, and droplets.

The conservation equations were solved numerically based on the finite-difference techniques. For the inverted annular flow region, a semi-implicit model was considered, while explicit models carried out computations for the wall, fully liquid, and dispersed flow regions. In the numerical model it was assumed that in the initial stages of the chill-down process the tube wall was cooled by nitrogen vapor only, and only after a specified period had elapsed the modeled four flow regimes were initiated. The calculated wall temperature for the lower elevations were higher than the experimental data.

The results of the present study together with the result of Kawaji and Banerjee[10,11] show that the two-fluid model used here is adequate for describing flow boiling phenomena. The model appears to be quite robust and applies to different classes of coolants including cryogenic liquids. Additional flow criteria are provided with this model, including line pressure variation with time which was not investigated in the present study. However, the major drawback of the specific model used is the requirement of knowing both the flow pattern as well as the quench front speed. This might be a heavy price to pay for the accuracy obtained, depending on the specific technology requirements. The model used can be quite readily adapted to different flow patterns with equal predictive capabilities.

The ultimate objective in this study is to develop a cryogenic quench predictive model for low gravity applications. The results obtained here are encouraging in that direction as long as the quench flow patterns sequence is known in a low-gravity environment. We are embarking on a series of low-gravity experiments at the present time aimed at defining this quench sequence.

References

[1]Kawaji, M., Ng, Y. S., Banerjee, S., and Yadigaroglu, G., "Reflooding with Steady and Oscillatory Injection: Part 1—Flow Regimes, Void Fraction, and Heat Transfer," *Journal of Heat Transfer*, Vol. 107, 1985, pp. 670–678.

[2]Burke, J. C., Byrnes, W. R., and Ruccia, F. E., "Pressurized Cooldown of Cryogenic Transfer Line," *Advances in Cryogenic Engineering*, Vol. 4, 1960, pp. 378–394.

[3]Bronson, J. C., Edeskuty, F. J., and Hammel, E. F., "Problems in Cooldown of Cryogenic Systems," *Advances in Cryogenic Engineering*, Vol. 7, 1960, pp. 198–205.

[4]Jacobs, R. B., "Liquid Requirements for the Cooldown of Cryogenic Equipment," *Advances in Cryogenic Engineering*, Vol. 8, 1962, pp. 529–535.

[5]Chi, J. W. H., "Cooldown Temperatures and Cooldown Time During Mist Flow," *Advances in Cryogenic Engineering*, Vol. 10, 1965, pp. 330–340.

[6]Steward, W. G., Smith, R. V., and Brennan, J. A., "Cooldown Transients in Cryogenic Transfer Line," *Advances in Cryogenic Engineering*, Vol. 15, 1970, pp. 354–362.

[7]Srinivasanof, K., Seshagiri, V., and Krishna Murthy, M. V., "Analytical and Experimental Investigation on Cool-Down of Short Transfer Lines," *Cryogenics*, Vol. 14, 1974, pp. 489–494.

[8]Chan, A. M. C., and Banerjee, S., "Refilling and Rewetting of a Hot Horizontal Tube. Part I: Experiments," *Journal of Heat Transfer*, Vol. 103, 1981, pp. 281–286.

[9]Chan, A. M. C., and Banerjee, S., "Refilling and Rewetting of a Hot Horizontal Tube. Part II: Structure of a Two-Fluid Model," *Journal of Heat Transfer*, Vol. 103, 1981, pp. 287–292.

[10]Kawaji, M., and Banerjee, S., "Application of a Multifield Model to Reflooding of a Hot Vertical Tube: Part 1—Model Structure and Interfacial Phenomena," *Journal of Heat Transfer*, Vol. 109, 1987, pp. 204–211.

[11]Kawaji, M., and Banerjee, S., "Application of a Multifield Model to Reflooding of a Hot Vertical Tube: Part II—Analysis of Experimental Results," *Journal of Heat Transfer*, Vol. 110, 1988, pp. 710–720.

[12]McGee, T. L., "An Experimental Study of a Vertical Cooldown Line with LN2," M.S. Thesis, Univ. of Tennessee, TN, 1990.

[13]Ganic, E. N., and Rohsenow, W. M., "Dispersed Flow Heat Transfer," *International Journal of Heat and Mass Transfer*, Vol. 20, 1977, pp. 855–866.

[14]Laverty, W. F., and Rohsenow, W. M., "Film Boiling of Saturated Nitrogen Flowing in a Vertical Tube," *Journal of Heat Transfer*, Vol. 89, 1967, pp. 90–98.

[15]Ishii, M., "Two-Fluid Model for Two-Phase Flow," *Multiphase Science and Technology*, edited by G. F. Hewitt, J. M. Delhaye, and N. Zuber, Vol. 5, Hemisphere, New York, 1990, pp. 1–63.

[16]Banerjee, S., and Chan, A. M. C. "1980 Flow Models—I, Analysis of the Averaged and Local Instantaneous Formulations," *International Journal of Multiphase Flow*, Vol. 6, 1980, pp. 1–24.

[17]Forslund, R. P., and Rohsenow, W. M., "Dispersed Flow Film Boiling," *Journal of Heat Transfer*, Vol. 90, 1968, pp. 399–407.

[18]Lee, K., and Ryley, D. J., "Evaporization of Water Droplets in Superheated Steam," *Journal of Heat Transfer*, Vol. 90, 1968, pp. 445–451.

[19]Papell, S. S., and Hendricks, R. C., "Incipience and Convective Boiling of Neon and Nitrogen," *Advances in Cryogenic Engineering*, Vol. 23, 1978, pp. 284–294.

[20]Bergles, A. E., and Rohsenow, W. M., "Determination of Forced-Convection Surface Boiling Heat Transfer," *Journal of Heat Transfer*, Vol. 86, 1964, pp. 365–372.

[21]Frost, W., and Dzakowic, G. S., "Extension of the Method of Predicting Incipient Boiling on Commercially Finished Surfaces," American Society of Mechanical Engineers/American Inst. of Chemical Engineers Paper 67-HT-61, 1967.

[22]Giarratano, P. J., and Smith, R. V., "Study of Forced Convection Boiling Heat Transfer Correlations for Cryogenic Fluids," *Advances in Cryogenic Engineering*, Vol. 11, 1965, pp. 492–506.

[23]Hedayatpour, A., "Transient Two-Phase Flow of Cryogenic Fluid in a Vertical Transfer Line During the Cooldown Process," Ph.D. Dissertation, Univ. of Tennessee, TN, 1990.

[24]Hinze, J. O., "Fundamentals of the Hydrodynamic Mechanism of Splitting in Sprays," *Industrial and Engineering Chemistry*, Vol. 43, 1951, pp. 1317–1324.

[25]Kays, W. M., *Convective Heat and Mass Transfer*, McGraw-Hill, New York, 1980.

[26]Sun, K. H., Gonzalez-Santalo, J. M., and Tien, C. L., "Calculations of Combined Radiation and Convection Heat Transfer in Rod Bundles Under Emergency Cooling Conditions," *Journal of Heat Transfer*, Vol. 98, 1976, pp. 414–420.

[27]Rowe, R. N., "Drag Forces in a Hydraulic Model of a Fluidized Bed—Part II," *Transactions Institute of Chemical Engineers*, Vol. 39, 1961, pp. 175–180.